

Noncontact, nondestructive elasticity evaluation of sound and demineralized human dental enamel using a laser ultrasonic surface wave dispersion technique

Hsiao-Chuan Wang

Simon Fleming

University of Sydney
Institute of Photonics and Optical Science
School of Physics
Sydney, New South Wales 2006
Australia

Yung-Chun Lee

National Cheng Kung University
Department of Mechanical Engineering
1 University Road
Tainan City 70101
Taiwan

Susan Law

University of Sydney
Institute of Photonics and Optical Science
School of Physics
Sydney, New South Wales 2006
Australia

Michael Swain

University of Sydney
Faculty of Dentistry
Sydney, New South Wales 2006
Australia

Jing Xue

Sichuan University
Faculty of Dentistry
Sydney, New South Wales 2006
Australia
and
Sichuan University
State Key Laboratory of Oral Diseases
Chengdu 610041
China

1 Introduction

Dental caries (tooth decay or lesion) is one of the most predominant diseases to afflict mankind. It is initiated by excessive mineral dissolution of the dental enamel caused by plaque bacteria induced acid,^{1,2} known as demineralization. Identifying caries at an early stage would allow minimally invasive reparative approaches, such as enhanced remineralization using fluoride, to inactivate the decay process or even repair the affected tooth structure. However, current clinical

Abstract. Laser ultrasonic nondestructive evaluation (NDE) methods have been proposed to replace conventional *in vivo* dental clinical diagnosis tools that are either destructive or incapable of quantifying the elasticity of human dental enamel. In this work, a laser NDE system that can perform remote measurements on samples of small dimensions is presented. A focused laser line source is used to generate broadband surface acoustic wave impulses that are detected with a simplified optical fiber interferometer. The measured surface wave velocity dispersion spectrum is in turn used to characterize the elasticity of the specimen. The NDE system and the analysis technique are validated with measurements of different metal structures and then applied to evaluate human dental enamel. Artificial lesions are prepared on the samples to simulate different states of enamel elasticity. Measurement results for both sound and lesioned regions, as well as lesions of different severity, are clearly distinguishable from each other and fit well with physical expectations and theoretical value. This is the first time, to the best of our knowledge, that a laser-based surface wave velocity dispersion technique is successfully applied on human dental enamel, demonstrating the potential for noncontact, nondestructive *in vivo* detection of the development of carious lesions. © 2009 Society of Photo-Optical Instrumentation Engineers. [DOI: 10.1117/1.3253396]

Keywords: biomedical inspection; nondestructive evaluation; laser ultrasonics; surface acoustic waves; remote sensing; fiber optics sensors; dental enamel evaluation.

Paper 09258R received Jun. 21, 2009; revised manuscript received Aug. 27, 2009; accepted for publication Aug. 31, 2009; published online Oct. 30, 2009.

treatment for dental caries is still dominated by invasive surgical interventions due to the fact that conventional diagnostic tools/techniques, such as tactile and x-ray assessments,³ are ineffective for quantifying the severity of the demineralization sites and detecting caries at an early stage. Specifically, these diagnostic methods are incapable of providing quantitative evaluation of the elastic modulus, which has been demonstrated to be directly linked to the level of mineralization, of dental enamel.⁴⁻⁶ Currently, for dental research purposes, nanoindentation is widely used for measuring the elastic modulus of dental hard tissue.^{5,7} Although it is able to make

Address all correspondence to: Hsiao-Chuan (David) Wang, University of Sydney, Institute of Photonics and Optical Science, School of Physics, Sydney, NSW 2006 Australia. E-mail: david.wang@usyd.edu.au

direct measurements, the indentation method involves contact destructive probing and can only be performed on extracted teeth (*in vitro* measurements). In this regard, a noncontact and nondestructive technique that could potentially provide localized *in vivo* evaluation of the elastic modulus of human dental enamel is desired.

A surface acoustic wave (SAW) is one type of elastic ultrasound that propagates on a sample surface, with its velocity governed by the elastic parameters of the layers it probes. In a complex inhomogeneous structure, such as a two-layer system, the wave is dispersed (its velocity varies with frequency). Determining the velocity at different frequencies yields a dispersion spectrum whose slope and curvature contain information about the elastic and geometric parameters of the material system. The SAW dispersion technique has been extensively utilized in the field of nondestructive evaluation (NDE) for determining the elastic modulus of surface materials and thin films,^{8–12} and could thus be useful to evaluate human dental enamel.

Conventional methods to generate and detect the SAW are accomplished by means of contact transducers such as piezoelectric materials. These devices are well established but are impractical for measurements on small objects due to their contacting nature and size. Over the last few decades, laser-based ultrasonic techniques have surpassed contact transducers to provide high-spatial-resolution remote measurements on curved or rough surfaces.^{13,14} The optical generation of SAW is relatively straightforward; in this study we irradiate the sample surface with short-duration laser pulses focused into a thin line by a cylindrical lens. The setup is simple and the laser pulse energy can be maintained at a low level for nondestructive operation. Optical detection of the typically nanometer or subnanometer amplitude SAW needs to be precise for the subsequent calculation of material constants. Laser interferometry is a very sensitive method for measuring ultrasonic surface displacement.^{15,16} Michelson and other free-space interferometers have been utilized to measure elastic ultrasound, but they have limited maneuverability, and critical alignment of the optics can be tedious and inappropriate for many areas of practical deployment.¹³ Optical fiber provides considerable practical advantages when used as the light steering medium of the interferometer, since no critical alignment of sensitive optics in the vicinity of the target is required.¹⁷ Furthermore, the flexibility and miniature size of the optical fiber can improve the ability of the interferometer to access areas that are difficult to examine with standard optics.^{18,19} Different designs of optical fiber interferometers (OFIs), such as Fabry-Perot²⁰ and Sagnac,²¹ have been demonstrated, but they require excessive auxiliary components such as fiber pig-tailed microlenses, phase modulators, and polarization controllers to optimize performance. In this study a simplified OFI that is easy to implement and control for high-frequency SAW measurements with minimum supporting components is described.

We present a laser ultrasonic system that allows surface material evaluation on small dimension samples through SAW dispersion analysis. The system performance and accuracy is first demonstrated by measurements on various metal structures. This is followed by the novel application to evaluate localized areas of extracted human tooth surface. Artificial

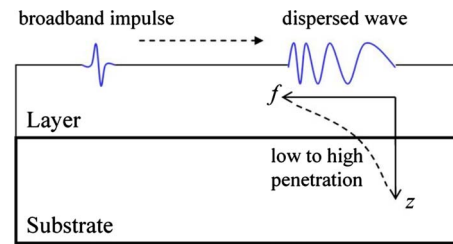


Fig. 1 Surface wave dispersion in a two-layer system.

lesions were prepared and both sound and decayed regions, as well as lesions of different severity, were measured. The experimental results are presented and discussed. For the first time, to the best of our knowledge, quantitative evaluation of the elasticity of sound and lesioned enamel using such a system is presented.

2 Laser Ultrasonic Nondestructive Evaluation Technique

A detailed description and more extensive testing results of this laser ultrasonic NDE technique can be found in a previous publication.²² In this work we only present material that is most relevant to this study.

2.1 Acoustic Theory

The wave energy of a SAW, and hence the wave motion, is concentrated within a penetration depth similar to its wavelength λ , beyond which the wave amplitude quickly becomes negligible.²³ This essentially means that the SAW velocity c_R is governed by the elastic constants of the material depth it probes. The SAW penetration depth z can be estimated from the relation:

$$z \approx \lambda = c_R/f, \quad (1)$$

where f is the signal frequency.

In an isotropic homogeneous medium, c_R is independent of the signal frequency as well as the propagation direction.²⁴ For a multilayer medium of different elastic properties, the wave propagation is influenced by all the layers it probes, such that c_R is governed by a generalized dispersion equation.²⁵ To understand the dispersion effect, consider a broadband surface wave propagating in the x_1 direction on a sample consisting of a substrate coated with an upper layer that has a lower SAW velocity, as shown in Fig. 1. Such a medium is of direct interest to our study, since a human tooth can be considered as a two-layer system within the scope of our intended investigation.

A broadband SAW impulse can be regarded as the superposition of surface waves with different frequencies. Referring to Fig. 1, the higher frequency components have a shallow penetration depth and are more influenced by the surface layer, traveling with a relatively slower velocity, whereas the lower frequency components penetrate deeper and are influenced more by the substrate elastic parameters. Thus the phase velocity c_R becomes a function of frequency and the SAW impulse is dispersed as it propagates.

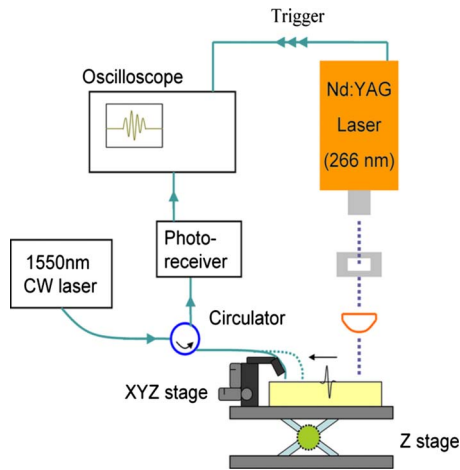


Fig. 2 Arrangement of the laser NDE system and the SAW dispersion measurement.

2.2 System Configuration

The schematic of the laser NDE system for SAW measurements is illustrated in Fig. 2.

A solid-state quadrupled Nd:YAG laser, operating at 266 nm, was used to excite the surface wave. The source laser pulses, with ~ 5 -ns duration, were directed through a rectangular mask and focused into a thin line by a cylindrical lens onto the sample surface (shown on the right of Fig. 2). The generated SAW propagates perpendicular to the line source and contains a wide frequency bandwidth enabling the signal to probe multiple layers in the material simultaneously, which is desired for the SAW dispersion measurement.

In our measurement setup, test objects were placed on a manual Z-stage for adjusting the separation between the lens and the sample, and hence the line-source width (defocusing the image). Reducing the line width can further increase the bandwidth of the generated SAW, but this inevitably raises the irradiating power density and may damage the specimen surface. During measurements, the laser pulse energy and the sample surface were constantly monitored to ensure no physical damage.

Detection of the ultrasound was performed by the OFI (shown on the left of Fig. 2) consisting of a 1550-nm continuous-wave laser as the light source, a three-port optical fiber circulator, and a photoceiver. These three components were joined using fiber connectors. The detected signal was averaged 32 times and displayed on a digital oscilloscope with a trigger signal from the Nd:YAG laser.

The tip of the middle port fiber of the circulator was cleaved to act as the probe head and placed on a micron-precision three-axis (xyz) positioning stage, such that the probe-to-sample separation can be adjusted to optimize the returning signal strength and the spatial resolution, as well as make measurements at different locations. This positioning stage permits measurements between 1 and 12 mm from the line source, with 0.01-mm precision. All measurements were made with a probe-to-sample separation of 5 mm or smaller.

The basic principle of this OFI is similar to a reference beam interferometer. The coherent laser light from the source I_0 was coupled into the circulator. As I_0 reaches the end of the

middle port fiber (sensing tip), about 4% of the light will be internally (Fresnel) reflected at the silica/air interface and serves as the reference beam I_1 . The rest of the light is incident on the sample surface, and then reflection causes a small portion of it I_2 to be coupled back into the fiber and become the measurement beam. Throughout the rest of the system, I_1 and I_2 copropagate toward the third port, and this essentially common path environment means that the path difference of the two beams, and hence their relative phase, depends only on the separation between the fiber tip and the sample surface. In a typical ultrasonic measurement, the phase modulation is less than π , which means that the elastic wave vibration amplitude is less than a quarter of the OFI source wavelength, and the interference intensity becomes a very good measure of the absolute acoustic waveform. However, the measured interference signal does not contain information about the absolute ultrasonic wave amplitude, since we did not have the means to know precisely the initial static phase difference (equivalent to controlling the probe-to-sample separation on a nanometre scale).

A more detailed discussion about the OFI can be found in Ref. 22.

2.3 Determination of the Experimental Dispersion Spectrum

To determine the experimental dispersion curve, generated surface waves were measured at various locations along the epicentral axis of the line source. The recorded wave signals were digitally bandpass filtered (1 to 50 MHz) to reduce the low and high frequency noise. Two signals, at locations x_1 and x_2 , were selected for dispersion analysis. They were cross-correlated to identify and exclude the noise signals, and then Fourier transformed. The phase difference between the ultrasonic signals $\varphi(f)$ was determined from the phase angle of the Fourier spectrum, from which the frequency-dependent SAW velocity can be determined using:

$$c(f) = 2\pi f \frac{x_2 - x_1}{\varphi(f)}. \quad (2)$$

The magnitude of the Fourier spectrum was used to identify the upper limit of the reliable frequency bandwidth with sufficient signal-to-noise ratio for accurate analysis results.^{22,26} The lower limit of the reliable bandwidth was chosen to be around 1 MHz, as signals of lower frequencies contain less information about the surface and suffer from low frequency ambient noise.

2.4 Validation Measurements on Common Metals

Prior to applying this system for evaluating human dental enamel, the capability of our system for measuring different types of surface waves (both nondispersed and dispersed) was investigated. In addition, the accuracy of the analysis technique for determining the experimental SAW dispersion spectrum must be tested by comparing with theoretical expectations. In this section we present results of evaluating different metal structures, and demonstrate the performance of the NDE technique. More extensive validation results of this system can be found in Ref. 22.

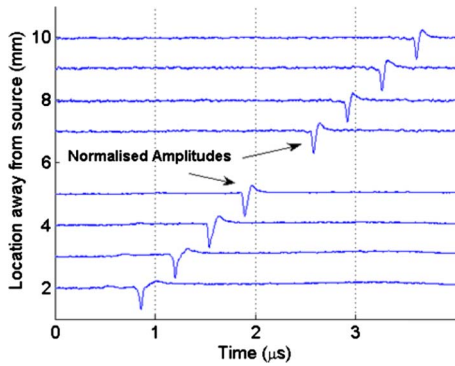


Fig. 3 Surface waves on the aluminium sample measured at different distances from the source. (The traces are identically scaled arbitrary units; see text for details.)

Homogeneous isotropic materials, namely aluminium and brass blocks, with known SAW velocities were measured [aluminium $\sim 2950 \text{ ms}^{-1}$, brass $\sim 1970 \text{ ms}^{-1}$ (Ref. 27)]. Figure 3 shows the surface waves on the aluminium sample measured at various locations between 2 and 10 mm from the line source with 1-mm step size. Note that the wave amplitudes are normalized, and that the y axis is not the scale of the traces but rather it serves only as a label to indicate for each trace the relevant location from the line source. The absence of waveform broadening indicates that no dispersion occurs in this homogeneous medium.

Signals measured at 2 and 10 mm from the line source were chosen and analyzed as discussed earlier. Surface wave phase velocity as a function of frequency was calculated using Eq. (2) and is displayed in Fig. 4. The same measurement was performed on the brass block, and the determined velocity is plotted also in Fig. 4. The signal-to-noise ratios for these sets of measurements were very high, such that the reliable frequency bandwidth extends to 30 MHz (demonstrated by the expected stable velocity value).

These experimental results for both homogeneous block materials match very well with the theoretical values (less than 1% difference), and they demonstrate, as expected, that no dispersion occurred in these uniform media.

For the study of a dispersive two-layer system, a sample composed of a $\sim 40\text{-}\mu\text{m}$ -thick nickel film sputtered onto a

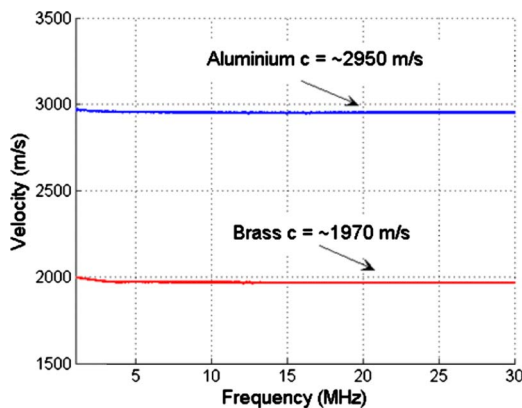


Fig. 4 Experimental SAW velocities for aluminium and brass samples.

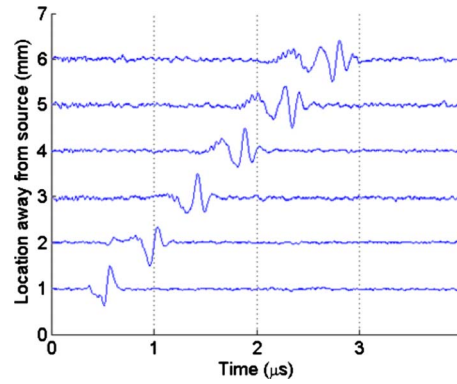


Fig. 5 Surface waves on a two-layer system of Ni film on glass substrate measured at locations 1 to 6 mm away from the source. (Y-axis as per Fig. 3.)

thick fused quartz glass substrate was used. The SAW velocities of the materials were known (nickel: $c_R \sim 2700 \text{ ms}^{-1}$; glass: $c_R \sim 3400 \text{ ms}^{-1}$). Figure 5 shows the surface waves measured along the propagation path up to 6 mm away from the line source with 1-mm spacing. The distortion of the acoustic waveform is apparent, and in this case it is obvious that the low frequency components, more influenced by the glass substrate, travel faster.

Signals with the furthest separation were once again chosen and cross-correlated for the dispersion analysis. In this measurement the reliable frequency bandwidth spanned from 1 to 20 MHz. The experimental dispersion curve is plotted in Fig. 6. To confirm the thickness of the nickel film, and hence the accuracy of the experimental result, the partial wave technique presented in Ref. 25 was used to calculate the theoretical SAW dispersion spectra using known parameters of the two substances with different film thicknesses (30, 40, and $50 \mu\text{m}$), also displayed in Fig. 6. Note that the local minimum of the theoretical dispersion curve shifted toward higher frequency as the thickness of the surface layer reduces. The experimental curve clearly fits best with the $40\text{-}\mu\text{m}$ simulation. The actual thickness of the nickel film was then measured with an optical micrometer and found to be $42 \pm 2 \mu\text{m}$ (it was not a perfectly uniform film).

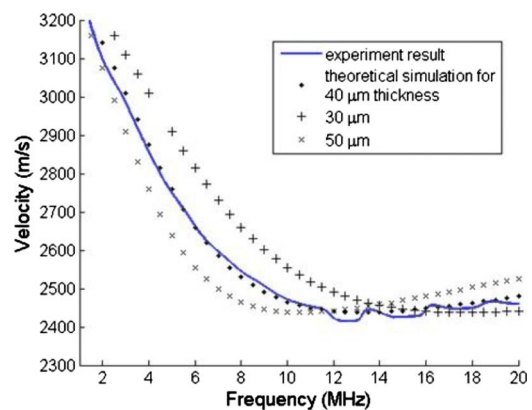


Fig. 6 Experimental and theoretical dispersion curves for nickel film on glass substrate.

The prior measurements demonstrate that our optical NDE system can generate and detect different types of surface waves on various samples. Excellent matches were obtained in fitting the experimental dispersion curves with theoretical simulations. This demonstrates that the curvature and the trend of the experimental dispersion curve within the reliable bandwidth are accurate in terms of revealing the state of elasticity of the medium in which the SAW propagates, most importantly the elastic response as a function of depth. The main source of uncertainty in the current implementation of this technique will most likely be the error in measuring the signal separations from the OFI translation stage manual micrometer adjustment.

3 Evaluation of Human Dental Enamel

3.1 Characteristics of Sound and Lesioned Enamel

Dental enamel envelops and protects the underlying dentin and is the hardest and the most mineralized substance of the human body. The unevenly distributed composition and the highly oriented microstructure of tooth enamel result in anisotropic and inhomogeneous mechanical and elastic properties.⁵ Kushibiki et al.²⁸ used line-focused-beam scanning acoustic microscopy (SAM) and measured the surface wave velocity as a function of propagation direction on the labial surface of extracted human incisors, and observed that the velocity values vary between about 3105 to 3155 ms⁻¹, with the maximum obtained in the direction parallel to the tooth axis (direction from crown to root). Peck, Rowe, and Briggs²⁹ repeated the investigation on the surface of human permanent molars using SAM and reported that the SAW velocity varied between about 3075 to 3142 ms⁻¹, with the maximum velocity also in the direction parallel to the tooth axis. The SAM technique has drawbacks in that the measuring steps can be tedious and lead to prolonged time requirements. Also, special polishing procedures for the specimens are a prerequisite that makes the technique impossible for clinical applications. In addition, it requires coupling fluid, whose physical conditions (e.g., temperature) need constant monitoring and maintaining.

An early caries lesion in enamel is observed clinically as a white opaque spot, and hence is referred to as a white spot lesion (WSL).³⁰ Within the enamel WSL, the surface layer is porous but remains relatively intact and mineral rich; however, the subsurface area under the WSL (the body of the lesion) is low in mineral (10 to 70% of the sound enamel). The WSL enamel thus has lower hardness and elastic modulus than that of sound enamel. The WSL layer on top of sound enamel essentially simulates a two-layer system similar to the one depicted in Fig. 1, thus dispersion is expected to occur in broadband signals propagating through a WSL area.

3.2 Sample Preparation and Artificial White Spot Lesion

Among the various teeth, it is advantageous to choose the incisor for initial studies because its front surface has the largest flat area of enamel. In addition, the enamel thickness is relatively constant (~1 mm) over a wide region near the center of the incisor front surface. This is desirable because the measured SAW dispersion will not depend significantly on the uneven thickness of the enamel layer, but rather on the

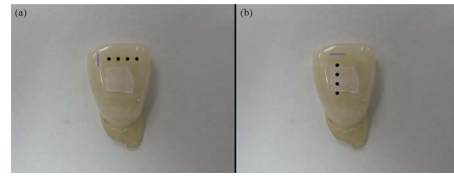


Fig. 7 Illustrations showing the positions of the SAW generation and detection on (a) the healthy region and (b) the WSL region of sample A.

elastic modulus variation. However, it is very unusual for a natural lesion to occur on the front surface of an incisor, and thus artificial lesions were created for this study. Artificial WSLs, may not be identical with natural enamel WSLs, but are widely used for dental research³⁰ and accepted as sufficiently similar. Two recently extracted sound human incisors were selected for the measurements (labeled A and B). Thin layers from the backs of the teeth were removed with a diamond blade so that the sample could be mounted on the measurement holder (on the Z-stage).

For artificial WSL preparation, the center region of the front incisor surfaces was abraded and polished approximately to a depth of ~100 μm below the natural surface with 400-grit abrasive papers. About ~70% of the front surface on both samples was polished, and the procedure was carefully performed such that very little of the enamel surface was removed so that the sample was still considered to be close to an *in vivo* condition. The samples were coated with a protective layer of nail varnish, while leaving windows of about 3 × 3 mm exposed in the polished regions, and then placed in prepared demineralization solution containing 2.2-mM Ca(NO₃)₂, 2.2-mM KH₂PO₄, and 50-mM acetic acid (pH=4.5).³¹ To produce lesions of different severity, sample A was soaked in the demineralization solution for five days, and sample B was treated for three days. After lesion treatment, the nail varnish was removed and the samples were rinsed with distilled water.

3.3 Measurements and Results

Prior to actual measurement, a study was conducted to determine the laser absorption spectrum of human enamel,³² and found that UV light was more efficiently absorbed than near-IR light, hence 266-nm emission from the Nd:YAG laser was chosen again to generate SAW. In addition, the laser damage threshold for enamel at 266 nm was experimentally determined. We used a tooth sample and irradiated it with a line source of laser pulse energy at ~1 mJ, and focused the line source gradually until thermal damage (predominately ablation) started to occur on the enamel surface. The corresponding line-source dimension was measured to be ~1.4 × ~0.02 mm, which gives a power density of ~7.5 × 10⁸ Wcm⁻². For our measurements on human dental enamel, presented next, we operated at a power density value that is below this estimated threshold with a margin such that all our experiments are nondestructive.

The first measurement was performed on the healthy region of sample A using the same system described before. Figure 7(a) shows how the healthy region of sample A was measured. Due to the limit in the usable sound enamel area,

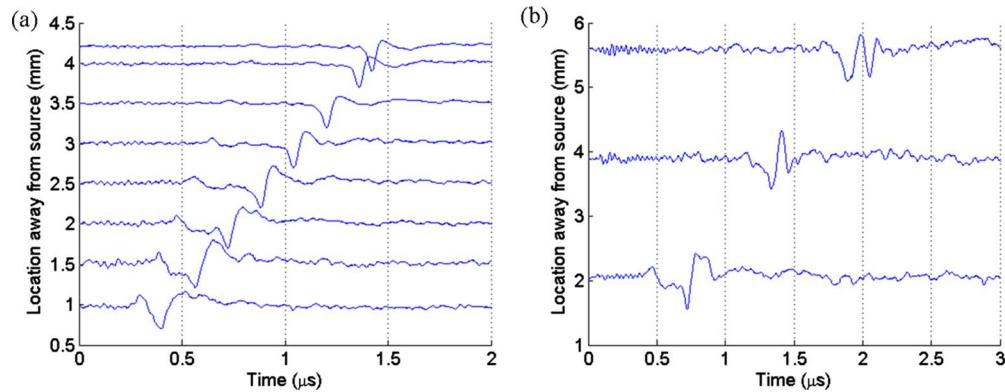


Fig. 8 Surface waves recorded at different locations from the line source on (a) sound and (b) WSL regions of sample A. (Y-axis as per Fig. 3)

the line source (illustrated as the line) was irradiated near the edge of the enamel surface and the SAW propagated in the direction horizontal to the tooth axis. The recording of the surface waves was made at several positions along the propagation path (illustrated as the dots). The measurement was repeated ten times and each time we shifted the sample position randomly by a small amount (± 0.2 mm) in the direction perpendicular to the wave propagation path, such that the final evaluation results were the averaged contribution from an area of rectangular shape with ~ 0.4 mm width. Recorded wave signals from one of the ten sound enamel measurements are presented in Fig. 8(a). The temporal shape of the surface waves appeared to be consistent during propagation.

For measurements on the WSL region, as illustrated in Fig. 7(b), we irradiated the line source near the top edge of the tooth and allowed propagation across the lesion in the direction parallel to the tooth axis. Surface waves were recorded at various locations, especially near the interface between the sound enamel and the WSL. Once again ten measurements, each with small random position variations, were repeated. Recorded wave signals from one set of the WSL measurements are shown in Fig. 8(b). We present the signals measured before entering the WSL (2 mm from source), near the center of the WSL (~ 4 mm from source), and just after the WSL (~ 5.7 mm from source). The change in the temporal wave profile clearly indicates that dispersion has taken place.

Two signals, with a separation of more than 2 mm, were selected from each measurement for the dispersion analysis. The dispersion analysis was performed as discussed before. The reliable bandwidth of both sound and lesioned enamel measurements were approximately 1 to 25 MHz.

Dispersion spectra of sound enamel and WSL measurements were calculated, and the ten-times-averaged values were used as the final results. These are presented in Fig. 9 with standard deviation error bars.

Several distinctive characteristics can be seen from the sample A results. In both sound enamel and WSL, the SAW velocities begin at a low value and increase with frequency. This can be explained by the influence of dentin, which has a much lower velocity value than enamel,^{33,34} on the surface wave propagation at low frequencies. For SAW with frequencies of 1 to 6 MHz, the corresponding probing depths are relatively deep, and the propagation structure for these low frequency components can be considered as a two-layer sys-

tem (sound bulk enamel on top of dentin). Dispersion is thus expected from the significant influence of the lower elastic modulus dentin.

In the sound enamel, once the SAW penetration depth is below a certain value (at ~ 6 MHz) at which the influence of dentin becomes negligible, the surface wave propagates in and probes only the enamel as a one-layer system. The velocity remains relatively constant at ~ 3150 ms^{-1} ; this value is very close to that previously reported.^{28,29} In the WSL region, the velocity begins to drop after 6 MHz and reaches a minimum of ~ 2840 ms^{-1} at ~ 16 MHz. The WSL dispersion profile after 6 MHz is similar to the result shown in Fig. 8, and thus confirms that the SAW propagation was influenced by the less elastic WSL layer (of unknown thickness at this stage) on top of the healthy bulk enamel. The differences between the two dispersion spectra are significant and clearly discriminate the two types of enamel.

The enamel anisotropy, as discussed in Sec. 3.1, is insignificant for this study, as previous studies^{28,29} demonstrated that the maximum SAW velocity on human enamel is obtained in the direction parallel to the tooth axis. This suggests that if the sound region measurements of the current study were also performed in the direction parallel to the tooth axis, a slightly higher velocity value would be obtained that could

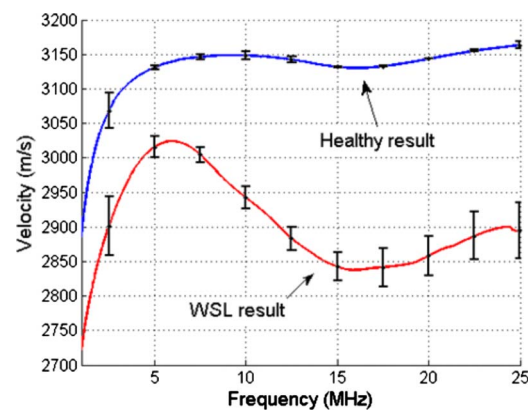


Fig. 9 Dispersion curves of the final averaged results from the sound region (blue) and WSL region (red) of sample A (5-day demineralization). (Color online only.)

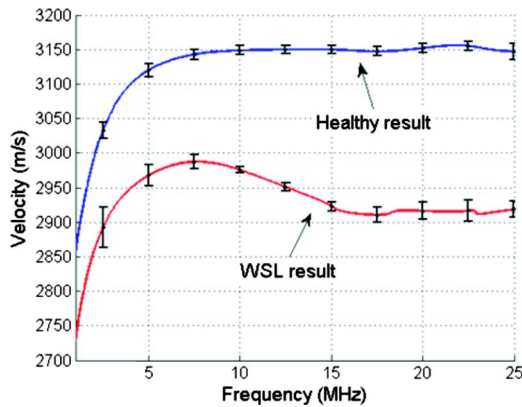


Fig. 10 Dispersion curves of the final averaged results from the enamel sound region (blue) and WSL region (red) of sample B (3-day demineralization). (Color online only.)

further discriminate the WSL and the sound enamel dispersion curves.

Sample B, with the three-day artificial lesion treatment, was measured in an identical manner to sample A discussed earlier. The measured waveforms and the reliable frequency bandwidth are similar to that of sample A and for brevity are not shown. The final averaged dispersion spectra, with standard deviation error bars, are shown in Fig. 10.

Comparing the results of samples A and B, one can first see that the sound enamel results share very similar dispersion profiles and velocity values, which indicates that the elasticity, as a function of depth, is similar between the two sound enamels. The WSL dispersion curves of both samples also have similar profiles, but there are a few important differences. For sample A the WSL curve has a minimum value of $\sim 2850 \text{ ms}^{-1}$, while the WSL curve for sample B has a slightly higher local minimum of $\sim 2910 \text{ ms}^{-1}$. This suggests that as expected the WSL of sample A, which has been demineralized for 5 days, is less elastic (a more severe lesion) than the sample B WSL that has been demineralized only for 3 days. In addition, the frequency at which the local minimum exists can help to provide insight into the thickness of the artificial lesion (for example, see Fig. 6). In sample A, the local minimum is at $\sim 16 \text{ MHz}$, while in sample B the local minimum is at 17 to 18 MHz. This indicates that the sample A lesion is thicker than the sample B lesion (due to prolonged demineralization) and influences the SAW propagation from a deeper probing depth (lower signal frequency). These results are very promising in terms of matching physical expectations regarding the surface wave propagation in enamel of different elasticity.

4 Conclusion

We present a remote laser ultrasonic system consisting of a laser line source for generating broadband SAW, and an optical fiber interferometer for detecting the ultrasound to provide nondestructive elasticity evaluation of the surface region of materials through surface wave dispersion analysis. Results from measuring common metal structures demonstrate the capability and accuracy of this NDE system. Measurements on

small dimension samples are made possible with the utilization of the fiber interferometer.

We apply this laser NDE technique, evaluate the enamel elasticity on the front surface of extracted human teeth, and obtain very promising results. In sound enamel regions, the SAW velocity matches well with values reported by previous researchers. In the artificial lesioned region, the velocity value is significantly lower, and the dispersion profile clearly discriminates between lesioned and sound enamel. In both regions the influence of the underlying dentin is observed as dispersion in the low frequency spectrum. Lesions of different severity are measured and from the dispersion curves, lesion layers of different elasticity and thickness are distinguishable. This is the first time that the elastic state, hence the level of mineralization, of human dental enamel has been evaluated using the laser SAW dispersion method, and the results demonstrate the potential of this laser NDE system to complement conventional dental examination methods for caries inspection.

Improvement on the usable bandwidth can be achieved by using laser pulses of shorter duration and a finer focusing lens to reduce the line-source width, hence increasing the signal strength at higher frequencies and expanding the usable band. Furthermore, utilizing an optical fiber laser, or optical fiber for laser delivery, for generating the ultrasound should permit future *in vivo* measurement.

Acknowledgments

This work was funded by the Australian Government and Bio-Dental Technology Pty. Ltd. under an ARC Linkage Grant, number LP0561184.

References

1. W. D. Miller, "Agency of micro-organisms in decay of the teeth," *Dental Cosmos* (1883).
2. B. Krasse, "Biological factors as indicators of future caries," *Int. Dent. J.* **38**, 219–225 (1988).
3. A. I. Ismail, "Visual and visuo-tactile detection of dental caries," *J. Dent. Res.* **83**, C56–C66, (2004).
4. F. Feagin, T. Koulourides, and W. Pigman, "The characterization of enamel surface demineralization, remineralization, and associated hardness changes in human and bovine material," *Arch. Oral Biol.* **14**(12), 1407–1417 (1969).
5. S. Habelitz, S. J. Marshall, G. W. Marshall Jr., and M. Balooch, "Mechanical properties of human dental enamel on the nanometre scale," *Arch. Oral Biol.* **46**(2), 173–183 (2001).
6. J. L. Cuy, A. B. Mann, K. J. Livi, M. F. Teaford, and T. P. Weihs, "Nanoindentation mapping of the mechanical properties of human molar tooth enamel," *Arch. Oral Biol.* **47**(4), 281–291 (2002).
7. F. Lippert, D. M. Parker, and K. D. Jandt, "In vitro demineralization/remineralization cycles at human tooth enamel surfaces investigated by AFM and nanoindentation," *J. Colloid Interface Sci.* **280**(2), 442–448 (2004).
8. *Ultrasonic Nondestructive Evaluation: Engineering and Biological Material Characterization*, T. Kundu, Ed., CRC Press, Boca Raton, FL (2004).
9. D. Schneider, B. Schultrich, H. J. Scheibe, H. Ziegele, and M. Griepentrog, "A laser-acoustic method for testing and classifying hard surface layers," *Thin Solid Films* **332**(1–2), 157–163 (1998).
10. C. Glorieux, W. Gao, S. E. Kruger, K. Van de Rostyne, W. Lauriks, and J. Thoen, "Surface acoustic wave depth profiling of elastically inhomogeneous materials," *J. Appl. Phys.* **88**(7), 4394–4400 (2000).
11. J. A. Rogers, A. A. Maznev, M. J. Banet, and K. A. Nelson, "Optical generation and characterization of acoustic waves in thin films: fundamentals and applications," *Annu. Rev. Mater. Sci.* **30**, 117–157 (2000).
12. Y. C. Lee, J. O. Kim, and J. D. Achenbach, "Measurement of elastic

- constants and mass density by acoustic microscopy," *Proc.-IEEE Ultrason. Symp.* **1**, 607–612 (1993).
13. C. S. Scruby and L. E. Drain, *Laser Ultrasonics: Techniques and Applications*, Adam Hilger Ltd., New York (1990).
 14. A. Neubrand and P. Hess, "Laser generation and detection of surface acoustic waves: Elastic properties of surface layers," *J. Appl. Phys.* **71**(1), 227–238 (1991).
 15. J. Monchalín, "Optical detection of ultrasound," *IEEE Trans. Ultrason. Ferroelectr. Freq. Control* **UFFC-33**(5), 485–499 (1986).
 16. R. J. Dewhurst and Q. Shan, "Optical remote measurement of ultrasound," *Meas. Sci. Technol.* **10**, R139–R168 (1999).
 17. B. Mitra, A. Shelamoff, and D. J. Booth, "An optical fibre interferometer for remote detection of laser generated ultrasonics," *Meas. Sci. Technol.* **9**, 1432–1436 (1998).
 18. A. J. A. Bruinsma and J. A. Vogel, "Ultrasonic noncontact inspection system with optical fiber methods," *Appl. Opt.* **27**(22), 4690–4695 (1988).
 19. T. D. Dudderar, C. P. Burger, J. A. Gilbert, J. A. Smith, and B. R. Peters, "Fiber optic sensing for ultrasonic NDE," *J. Nondestruct. Eval.* **6**(3), 135–146 (1987).
 20. H. S. Park, G. Thursby, and B. Culshaw, "Detection of laser-generated ultrasound based on phase demodulation technique using a fibre Fabry-Perot interferometer," *Meas. Sci. Technol.* **16**, 1261–1266 (2005).
 21. T. S. Jang, S. S. Lee, B. Kwon, J. Lee, and J. J. Lee, "Noncontact detection of ultrasonic waves using fiber optic sagnac interferometer," *IEEE Trans. Ultrason. Ferroelectr. Freq. Control* **49**(6), 767–775 (2002).
 22. H. C. Wang, S. Fleming, and Y. C. Lee, "A remote, non-destructive laser ultrasonic material evaluation system with simplified optical fibre interferometer detection," *J. Nondestruct. Eval.* **28**(2), 75–83 (2009).
 23. E. Soczkiewicz, "The penetration depth of the rayleigh surface waves," *Nondestr. Test. Eval.* **13**, 113–119 (1997).
 24. J. D. Achenbach, *Wave Propagation in Elastic Solids*, Elsevier Science Publishers B.V., New York (1984).
 25. J. L. Rose, *Ultrasonic Waves in Solid Media*, Cambridge University Press, Cambridge, UK (1999).
 26. D. Schneider and T. Schwarz, "A photoacoustic method for characterising thin films," *Surf. Coat. Technol.* **91**(1–2), 136–146 (1997).
 27. A. Briggs, *Acoustic Microscopy*, Clarendon Press, Oxford (1992).
 28. J. Kushibiki, K. L. Ha, H. Kato, N. Chubachi, and F. Dunn, "Application of acoustic microscopy to dental material characterization," *IEEE Trans. Ultrason. Ferroelectr. Freq. Control*, pp. 837–842 (1987).
 29. S. D. Peck, J. M. Rowe, and G. A. Briggs, "Studies on sound and carious enamel with the quantitative acoustic microscope," *J. Dent. Res.* **68**, 107–112 (1989).
 30. J. Arends and J. Christoffersen, "The nature of early caries lesions in enamel," *J. Dent. Res.* **65**(1), 2–11 (1986).
 31. J. M. ten Cate and P. P. Duijsters, "Influence of fluoride in solution on tooth demineralization. I. Chemical data," *Caries Res.* **17**(3), 193–199 (1983).
 32. H. C. Wang, S. Fleming, S. Law, and T. Huang, "Selection of an appropriate laser wavelength for launching surface acoustic waves on tooth enamel," *Proc. IEEE Australian Conf. Opt. Fibre Technol./Australian Opt. Soc.*, pp. 99–101, IEEE, Piscataway, NJ (2006).
 33. R. G. Maev, L. A. Denisova, E. Y. Maeva, and A. A. Denissov, "New data on histology and physico-mechanical properties of human tooth tissue obtained with acoustic microscopy," *Ultrasound Med. Biol.* **28**(1), 131–136 (2002).
 34. D. W. Blodgett, "Applications of laser-based ultrasonics to the characterization of the internal structure of teeth," *J. Acoust. Soc. Am.* **114**(1), 542–549 (2003).